53BP1 exchanges slowly at the sites of DNA damage and appears to require RNA for its association with chromatin

Fiona Pryde[1,*], Shirin Khalili[1,*], Kathryn Robertson[1], Jim Selfridge[2], Ann-Marie Ritchie[2], David W. Melton[2], Denis Jullien[1] and Yasuhisa Adachi[1,‡]

[1]The Wellcome Trust Centre for Cell Biology, The Institute of Cell and Molecular Biology, The University of Edinburgh, The King's Buildings, Edinburgh, EH9 3JR, UK
[2]Sir Alastair Currie Cancer Research UK Laboratories, Molecular Medicine Centre, The University of Edinburgh, Western General Hospital, Edinburgh, EH4 2XU, UK
*These authors contributed equally to this work
‡Author for correspondence (e-mail: y.adachi@ed.ac.uk)

Accepted 17 February 2005
Journal of Cell Science 118, 2043-2055 Published by The Company of Biologists 2005
doi:10.1242/jcs.02336

Summary

53BP1 protein is re-localized to the sites of DNA damage after ionizing radiation (IR) and is involved in DNA-damage-checkpoint signal transduction. We examined the dynamics of GFP-53BP1 in living cells. The protein starts to accumulate at the sites of DNA damage 2-3 minutes after damage induction. Fluorescence recovery after photobleaching experiments showed that GFP-53BP1 is highly mobile in non-irradiated cells. Upon binding to the IR-induced nuclear foci, the mobility of 53BP1 reduces greatly. The minimum (M) domain of 53BP1 essential for targeting to IR induced foci consists of residues 1220-1703. GFP-M protein forms foci in mouse embryonic fibroblast cells lacking functional endogenous 53BP1. The M domain contains a tandem repeat of Tudor motifs and an arginine- and glycine-rich domain (RG stretch), which are often found in proteins involved in RNA metabolism, the former being essential for targeting. RNase A treatment dissociates 53BP1 from IR-induced foci. In HeLa cells, dissociation of the M domain without the RG stretch by RNase A treatment can be restored by re-addition of nuclear RNA in the early stages of post-irradiation. 53BP1 immunoprecipitates contain some RNA molecules. Our results suggest a possible involvement of RNA in the binding of 53BP1 to chromatin damaged by IR.

Supplementary material available online at
http://jcs.biologists.org/cgi/content/full/118/9/2043/DC1

Key words: 53BP1, Ionizing radiation, DNA damage, FRAP, RNA

Introduction

Ionizing radiation (IR) produces a broad spectrum of damage in DNA, including base lesions and strand breaks (Ward, 1998). After exposure to IR, the proteins involved in repair and checkpoint signal transduction are recruited to specific nuclear locations or foci called IR-induced foci (IRIF). IRIF are thought to correspond to the sites of DNA double-strand breaks (Du et al., 2003; Melo et al., 2001; Mirzoeva and Petrini, 2001; Rogakou et al., 1999).

The focal phosphorylation of H2AX (γ-H2AX) and the assemblies of 53BP1 (p53 binding protein 1), HDAC4 and MDC1/NFBD1 foci occur within minutes of IR exposure (Anderson et al., 2001; DiTullio et al., 2002; Kao et al., 2003; Nelms et al., 1998; Rappold et al., 2001; Rogakou et al., 1999; Schultz et al., 2000). Later, BRCA1 and Mre11-Nbs1-Rad50 foci become more apparent (~40 minutes to hours after exposure, depending on the cell line). The assembly of IRIF involves some sequential dependency (Paull et al., 2000). In cells lacking H2AX, formation of the 53BP1, Nbs1 and BRCA1 foci is impaired (Bassing et al., 2002; Celeste et al., 2002). BRCA1 foci assembly does not occur in the absence of 53BP1 at a lower dose of IR (Fernandez-Capetillo et al., 2002; Wang et al., 2002). Precise analysis of early stages of post-IR showed that the transient recruitment of 53BP1, Nbs1 and BRCA1 to the sites of DNA damage occurs in the absence of H2AX but subsequent retention of these factors in the proximity of damaged DNA does not occur (Celeste et al., 2003; Du et al., 2003). This indicated that the initial recruitment and subsequent stable association of the factors on the damaged chromatin are two distinct processes.

53BP1 was originally identified in a yeast two-hybrid screen using the p53 tumor suppresser as bait. 53BP1 interacts with p53 through a tandem repeat of BRCT (BRCA1 C-terminus) motifs at its C-terminus (Derbyshire et al., 2002; Iwabuchi et al., 1994; Joo et al., 2002). The BRCT motif consists of ~95 amino acids and is found in a number of proteins involved in the DNA damage response (Bork et al., 1997). BRCT motifs mediate protein-protein interactions and in some cases bind specifically to phosphorylated targets (Dulic et al., 2001; Grawunder et al., 1998; Manke et al., 2003; Rodriguez et al., 2003; Soulier and Lowndes, 1999; Yu et al., 2003). In higher eukaryotes, three of the factors described above that play a role in DNA-damage-response- and checkpoint signalling, namely

53BP1, BRCA1 and MDC1/NFBD1, contain a tandem repeat of BRCT motifs at their C-terminus.

The C-terminus BRCT domains of 53BP1 show homology to those of checkpoint proteins Crb2 in fission yeast and Rad9 in budding yeast. Although Crb2 and Rad9 share little amino acid sequence similarity outside the BRCT domains, both are required for the activation of the downstream effecter kinases Chk1 and Chk2/Rad53, which are involved in DNA damage and/or replication checkpoint controls (Li et al., 2002; Mochida et al., 2004; Saka et al., 1997; Schwartz et al., 2002). In vertebrates, experiments with RNA interference and knockout mice have shown that 53BP1 is involved in DNA damage checkpoint partly through activation of Chk2 kinase (DiTullio et al., 2002; Fernandez-Capetillo et al., 2002; Wang et al., 2002). In *S. cerevisiae*, Rad9 functions catalytically to activate Rad53 protein kinase (Gilbert et al., 2001). Recent evidence indicates that Crb2 and 53BP1 may potentially regulate ATM-related kinases (Mochan et al., 2003; Mochida et al., 2004).

In this study, we examined the dynamics of 53BP1 before and after IR in live cells. 53BP1 is highly mobile before IR; however, after association with IRIF, the mobility decreases greatly. The minimum domain (M domain) of 53BP1, essential for foci targeting, consists of the central 483 residues, which lie outside the C-terminal BRCT domain. It contains an arginine- and glycine-rich stretch and two Tudor motifs, both of which are often found in proteins involved in RNA metabolism. The association of 53BP1 to the IRIF is sensitive to ribonuclease treatment. The results suggest that an RNA component is involved in the assembly of 53BP1 protein near the sites of DNA damage.

Materials and Methods

Plasmid construction

All the EGFP:m53BP1 fusion constructs used in transfections were made in pEGFP-C1 or pEGFP-N1 (Clontech). The details of the construction have been described previously (Jullien et al., 2002). The DNA sequences to be fused were amplified by PCR using a polymerase with proofreading activity (Vent®, Promega) and cloned into appropriate expression plasmids through introduced restriction enzyme cutting sites. The internal deletion constructs (ΔTUD, ΔRG, ΔXe) and the SQ motif mutants (Ser to Ala codon conversion) were made using the Exsite PCR-based Site-directed Mutagenesis kit (Stratagene). All the constructs were verified by sequencing.

Immunofluorescence staining

Immnofluorescence staining was performed as described previously (Anderson et al., 2001). Affinity purified anti-human or anti-mouse 53BP1 (Anderson et al., 2001; Jullien et al., 2002) antibodies were used at a concentration of 10 μg/ml. Anti-phospho-H2AX monoclonal antibodies and anti-Chk2T68P antibodies were purchased from Upstate Cell Signaling Solutions and Cell Signaling Technology, respectively. Antibody concentrations were used as recommended by the manufacturer (usually, 10 μg/ml for staining). For double-labelling with GFP, anti-mouse IgG-Cy3 (Amersham Pharmacia Biotech) antibodies were used as secondary antibodies. Cells were mounted in medium containing DAPI (Vectashield). Images were recorded using a Zeiss Axioskop microscope equipped with a VYSIS image recording system or a Zeiss Axiovert 200 controlled by SlideBook 3.0 from Intelligence Imaging Innovations (3I).

Transfection, X ray-irradiation and RNAse treatment

MEF, HeLa or NIH3T3 cells were grown in DMEM plus 10% fetal bovine serum and transiently transfected by calcium phosphate precipitation or using LipofectAmine Plus™ Reagent (GibcoBRL). For calcium phosphate precipitation, 1 μg DNA was precipitated and applied onto the cells grown on coverslips (22×22 mm) for 14 hours. Coverslips were then washed with PBS, supplied with fresh DMEM media and incubated for 16-24 hours to allow expression of the GFP-fusion proteins. For lipofection, 0.25 μg DNA (or 1 μg for NIH3T3 and MEFs) was used. Cells were irradiated with 10 Gy of X-rays and incubated for 1-2 hours to allow 53BP1 foci formation. For RNAse experiments, cells were permeabilized (0.5% or 2% Tween 20 in PBS for 10 minutes) and treated with or without 1 mg/ml RNase A in 70 μl of PBS for 15 minutes at room temperature. Five units of RNase H (Sigma) were applied per cover glass. After RNase digestion, some of the samples were washed with PBS, treated with 40 units of RNase inhibitor and then incubated with 2 μg nuclear RNA, or the same amount of tRNA, for 30 minutes at room temperature. The samples were fixed with methanol/acetone. Similar results were obtained by formaldehyde fixation (data not shown).

Stable transfection of pEGFP-m53BP1 in HeLa cells

Three micrograms of a construct expressing the full-length mouse 53BP1 gene fused to GFP (EGFP:m53BP1) (Jullien et al., 2002) was used to transfect HeLa cells in a 60 mm dish by calcium phosphate precipitation. Transfection efficiency was monitored under a fluorescence microscope. The medium was changed 12 hours after transfection. At 24 hours post-transfection, the cells were trypsinised, resuspended in fresh medium, and counted using a haemocytometer. Serial dilutions were seeded into five 96-well plates. From this point onward, the medium was supplemented with 50 μg/ml neomycin. Neomycin-resistant cells were trypsinised from confluent wells and seeded onto progressively larger tissue culture dishes until stocks of confluent 75 cm^2 flasks could be made. Cells from each stock were then cultured on a cover glass in a 35 mm dish, exposed to 10 Gy IR, allowed to recover for 1-2 hours, fixed, mounted onto slides, and observed under the microscope. The stock producing green nuclear foci in 9 out of 10 cells was further propagated and used in this study.

Live cell imaging, micro-irradiation, and FRAP

All live cell imaging experiments were performed on cells grown in 35 mm glass-bottom dishes (Iwaki) in DMEM without Phenol Red (BioWhitaker). Immediately prior to microscopy, the medium was supplemented with 10 mM Hepes-NaOH (pH 7.5). The dish was placed into a BC-250A bionomic cell (20/20 Technologies) and kept at 37°C during imaging. Additionally, the 63× objective lens used was maintained at 37°C with a Zeiss Objective Heater regulated by a Tempcontrol 37-2 digital controller. Image capture and analysis was performed using Slidebook 4.0 from Intelligent Imaging Innovations, Inc.

A Spectraphysics (model 337201-01) nitrogen pulse laser (337 nm), excited by 5 mM Coumarin to emit photons at approximately 440 nm, was used at various settings to determine experimentally the power level needed for induction of DNA damage in the nuclei of GFP-m53BP-expressing HeLa cells. DNA damage was manifested by targeted accumulation of GFP-m53BP1 in a nucleus exposed to the laser. Settings used for photobleaching alone were tested to verify a lack of targeted accumulation. Settings used for photobleaching and micro-irradiation corresponded to 0.67% and 5.8% laser transmission, respectively.

For micro-irradiation, MEF cells were transiently transfected with GFP-m53BP1 or GFP-M. A pre-treatment image was captured, after which a narrow rectangular region of the nucleus was subjected to micro-irradiation, and imaged immediately after the treatment.

Subsequent images were captured every 30 seconds (GFP-m53BP1) for 10 minutes, or 60 seconds (GFP-M) for 20 minutes. All captured images were single-plane exposures of 0.1 s.

For FRAP experiments of GFP-m53BP1 IRIF, stably transfected HeLa cells were exposed to 10 Gy of IR and allowed to recover for 1 hour at 37°C with supplemented 5% CO_2. An initial stack of images was taken in z-planes 1 μm apart. After the first stack of images was taken, one of the nuclear IRIF was photobleached. Immediately after the photobleaching event, a new stack of images was taken, and the imaging was performed every 60 seconds for 30 minutes. A projection image was created from each stack of images, and these projections were used to make a time-lapse record of events. The percentage of fluorescence recovery of the photobleached IRIF was calculated at each time point with the following formula: $R_t=(F_t\times N_i)/(F_i\times N_t)$, where R is the fraction of the original IRIF fluorescence, F is the average fluorescence of the IRIF minus the average background fluorescence, N is the average fluorescence of the entire nucleus minus the average background fluorescence, t is the time point for which the calculation is being performed, and i is the initial value prior to photobleaching.

FRAP experiments on GFP and GFP-m53BP1 in non-irradiated cells were performed at the Wellcome Trust Biocentre Light Microscopy Facililty, Dundee, UK, following the method of Andrews et al. (Andrews et al., 2004). HeLa cells transiently transfected with a plasmid expressing GFP fused to a nuclear localisation signal (pCDNA3 GFP:ICAD-$L^{312-331}$) (Samejima and Earnshaw, 2000) or HeLa cells stably transfected with EGFP:m53BP1 were grown on 42 mm glass coverslips (no. 1; Helmut Sauer). During FRAP experiments, cells were maintained at 37°C by use of a closed perfusion chamber (Bachofer) and subjected to a 10 mW, 488 nm solid-state laser fitted to a FRAP-enabled DeltaVision Spectris. All images were collected in 0.05 second exposures. After three pre-bleach images were obtained, a diffraction-limited spot was photobleached at 60% laser power for 0.2 seconds. Seven images were collected every 0.17 seconds starting at 0.002 seconds after photobleaching, followed by 6 images every 0.33 s, then 6 images every 0.84 s, and finally 31 images every 1.67 seconds. Fluorescence recovery was calculated as indicated above. The method of Axelrod (Axelrod et al., 1976) was used to calculate $t_{½}$ of GFP freely diffusing in the nucleus.

RNA procedures

HeLa cell nuclei were isolated in a polyamine buffer and nuclear extracts were prepared as described (Dignam et al., 1983; Lewis et al., 1984). Immunoprecipitation was performed essentially as described previously (Anderson et al., 2001). Nuclear extracts (from nuclei of 40 OD_{260}) were added with 200 μg of anti-53BP1 or normal rabbit IgG and 250 μl of protein A-Sepharose. After washing, beads were resuspended in 300 μl 50 mM Tris-HCl, pH 7.9, 10 mM EDTA, 150 mM NaCl, 1% SDS, 50 μg/ml proteinase K and incubated at 37°C for 30 minutes. The mixtures were extracted with an equal volume of phenol/chlorform/isoamylalcohol (125:24:1, pH 4.7). Nucleic acids were precipitated with 0.1 M sodium acetate, pH 4.0 and an equal volume of isopropanol. RNA was labeled with [5′-^{32}P]pCp (Keith, 1983). The labelled RNA was separated on a 6% polyacrylamide gel with 7 M urea and 16.7% formamide and autoradiographed.

Generation of 53BP1$^{-/-}$ mice

A fragment of the mouse 53BP1 cDNA encoding the C-terminal part of the protein was used to screen a mouse 129 genomic library (Stratagene). Analysis of several overlapping phage genomic inserts by restriction analysis, Southern blotting, and sequencing allowed the characterization of the structure of about 38 kb of the 3′ region of the mouse *53BP1* gene. The targeting vector contained a PGK-HPRT positive selection marker gene flanked by a 6 kb *Bam*HI 5′ homology fragment and a 2 kb 3′ homology region (supplementary material Fig. S1A). The 3′ homology region was upstream of a thymidine kinase negative selection marker to counter-select for non-homologous integration. The targeting vector was designed to replace the last 10 coding exons of the *m53BP1* gene (encoding 702 amino acids of the C-terminus of m53BP1 including the BRCT repeat, NLS and most of the targeting domain) with PGK-HPRT after homologous recombination. The targeting vector was linearized by *Not*I digestion and electroporated into ES cells. After appropriate positive and negative selection of transfectants, homologous recombination events were screened by Southern blotting with *Eco*RI digestion and by hybridization to a probe external to the 5′ homology region (supplementary material Fig. S1A). 53BP1$^{+/-}$ ES cells were then microinjected into blastocysts (C57BL/6) to generate chimeric mice, which transmitted the mutation into the mouse germline. Heterozygous 53BP1$^{+/-}$ mice were detected by Southern blotting performed on tail genomic DNA digested with *Eco*RI as described for ES cell screening. 53BP1$^{+/-}$ mice were intercrossed to generate homozygous targeted 53BP1 mice (supplementary material Fig. S1B). Mouse embryonic fibroblast cells were prepared from embryos at 11.5-12.5 days post-coitum (dpc). The HPRT-targeted mutant allele was determined by PCR using primers: 5′-AGCCTACCCTCTG-GTAGATTGTCG-3′ and 3′-GAAGGACGTAGAGACTCGGAAC-AA-5′.

Results

Dynamics of GFP-m53BP1 in living cells

Previously we showed that 53BP1 localises to the kinetochore of mitotic chromosomes by transient expression of GFP fused to full-length mouse (m) 53BP1 in HeLa cells (Jullien et al., 2002). This GFP-m53BP1 was used to study the response of 53BP1 to DNA damage in live cells. GFP-m53BP1 is homogenously distributed over chromatin in untreated cells (Fig. 1A, upper panels). After exposure to X rays it re-localises to ionising radiation-induced foci (IRIF) and co-localises with phosphorylated H2AX foci (Fig. 1A; γH2AX).

We established a stably transfected HeLa cell line that expresses GFP-m53BP1 (see Materials and Methods). Expression of full-length GFP-m53BP1 was confirmed by western blot with anti-GFP antibodies (Fig. 1B, lanes 1,2). The mobility of GFP-m53BP1 was slightly slower than that of endogenous 53BP1, although the fusion protein band was not resolved from the endogenous 53BP1 (note that all the samples shown in this figure were separated on the same gel). The anti-C-m53BP1 recognized a thicker band in the extracts of HeLa cells with GFP-m53BP1 than in control HeLa cell extracts (Fig. 1B, lane 5). The antibodies used in this experiment recognize human 53BP1 as well as mouse 53BP1 in western blots (compare lanes 3 and 4). Equal amounts of total protein were loaded in each lane. The stable cell line expresses a moderate level of GFP-m53BP1.

We followed the redistribution of GFP-m53BP1 after DNA damage induction by exposing cells to laser micro-irradiation (Limoli and Ward, 1993; Rogakou et al., 1999). The procedure was originally developed to induce double-strand DNA breaks by exposing cells to UVA in the presence of Hoechst dye 33258 after the incorporation of 5-bromo-2′deoxyuridine (BrdU) into cellular DNA (Limoli and Ward, 1993). Subsequently, UVA exposure was replaced with UVA (390 nm) pulsed laser to induce DNA damage at specific regions inside the nucleus (Lukas et al., 2003; Rogakou et al., 1998). During optimization of our experimental conditions, we found that exposure to

higher power laser can induce accumulation of GFP-m53BP1 at the laser-exposed subnuclear region without BrdU and Hoechst 33258 treatments (see Materials and Methods) (Rogakou et al., 1999). In Fig. 1C, a thin strip across the nucleus of a MEF (mouse embryonic fibroblast) cell expressing GFP-m53BP1 was irradiated with a pulse laser. This 'stripe' region of GFP-m53BP1 induced by the treatment probably contained a number of DNA lesions since phosphorylated H2AX colocalised with the GFP-m53BP1 stripe (Fig. 1C, γH2AX). Time-lapse image capturing showed that the visible accumulation of GFP-m53BP1 was apparent approximately 120 seconds after exposure to a pulse laser (Fig. 1D, upper panels; see also Movie 1 in supplementary material). The time scale of this rapid re-localisation was consistent with previous results for the endogenous 53BP1 in cells fixed after IR (Celeste et al., 2003; Schultz et al., 2000). The minimum domain (M) for targeting m53BP1 to IRIF is located in residues of 1220 to 1703 (see later section). The appearance of the GFP-M stripe at the laser-irradiated region took over 1000 seconds, which was slower than that of full-length GFP-m53BP1 (Fig. 1D, lower panels). The stripe was also less intense at this early stage of post-IR.

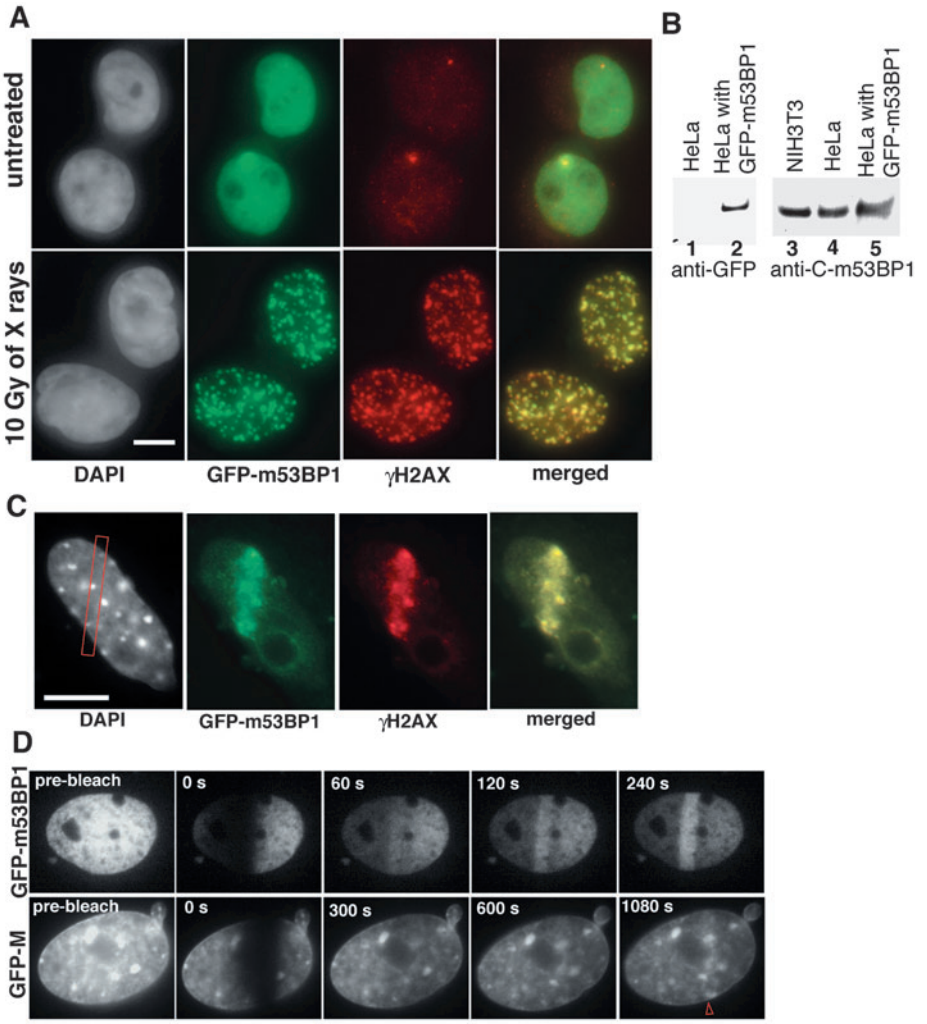

Fig. 1. Dynamics of GFP-m53BP1 in vivo. (A) HeLa cells stably expressing GFP fused to full-length mouse 53BP1 (GFP-m53BP1) were untreated or exposed to ionising radiation (IR; 10 Gy of X rays). After recovery for 1 hour, cells were fixed and stained for phosphorylated histone H2AX (γH2AX). (B) Extracts were prepared from the HeLa cell line stably expressing GFP-m53BP1 and analysed by western blotting with anti-GFP antibodies (lanes 1, 2) and with antibodies against the C-terminus of mouse 53BP1 (lanes 3,4,5). Equal amounts of extracts from mouse NIH3T3 cells (lane 3) and un-transfected HeLa cells (lanes 1, 4) were run as controls. Samples shown here were separated on the same gel. GFP-m53BP1 migrates slightly slower than the endogenous m53BP1, which makes the band in lane 5 broader than the band in lane 4. Note that the two proteins were not separable. (C) Accumulation of GFP-m53BP1 at the nuclear region damaged by high power laser. Wild-type MEF (mouse embryonic fibroblast) cells were transfected with GFP-m53BP1 and irradiated with a laser at the region indicated in red. After GFP-m53BP1 stripe formation, the cells were fixed and stained for phosphorylated (γ) H2AX with Cy3 (red). The bright spots stained with DAPI are condensed heterochromatin of mouse cells. (D) Time lapse recording of laser-induced stripe formation (the stripe is marked by an arrowhead). Wild-type MEF cells, transfected with GFP-m53BP1 or GFP-M, were micro-irradiated and maintained at 37°C. Sequential images were captured and used to create a movie series. Selected frames are shown, along with the corresponding time (in seconds) after micro-irradiation.

GFP-m53BP1 forms foci at sites of DNA damage and complements the phosphorylation defect in cells lacking endogenous 53BP1

We examined whether GFP-m53BP1 was functional in DNA-damage-checkpoint signal activation. Cells lacking 53BP1 do not form foci detected by antibodies that recognize Chk2 phosphorylated at Thr68 (Chk2T68P) after exposure to IR (Wang et al., 2002; Ward et al., 2003b). We examined the ability of the GFP-m53BP1 to restore the Chk2T68P focus formation in cells derived from mutant mice that lack functional 53BP1. The knockout mice produced in this study had a homozygous deletion of the last 10 exons of the 53BP1 gene, encoding 702 amino acids of the C-terminus of m53BP1 (residues 1255 to 1957; the full-length protein consists of 1957 amino acid residues), including the BRCT repeats, NLS, and most of the focus-targeting domain (see supplementary material Fig. S1). The homozygous mutant mice were viable and fertile, which is consistent with the published results from other laboratories (Fernandez-Capetillo et al., 2002; Morales et al., 2003; Ward et al., 2003b). Antibodies against the C-terminus of m53BP1 (residues 1293 to 1809) did not detect the protein in tissues and MEFs derived from the mutant mice (Fig. 2A,C left panel, –/–). Antibodies against the N-terminus 355 residues of m53BP1 detected a

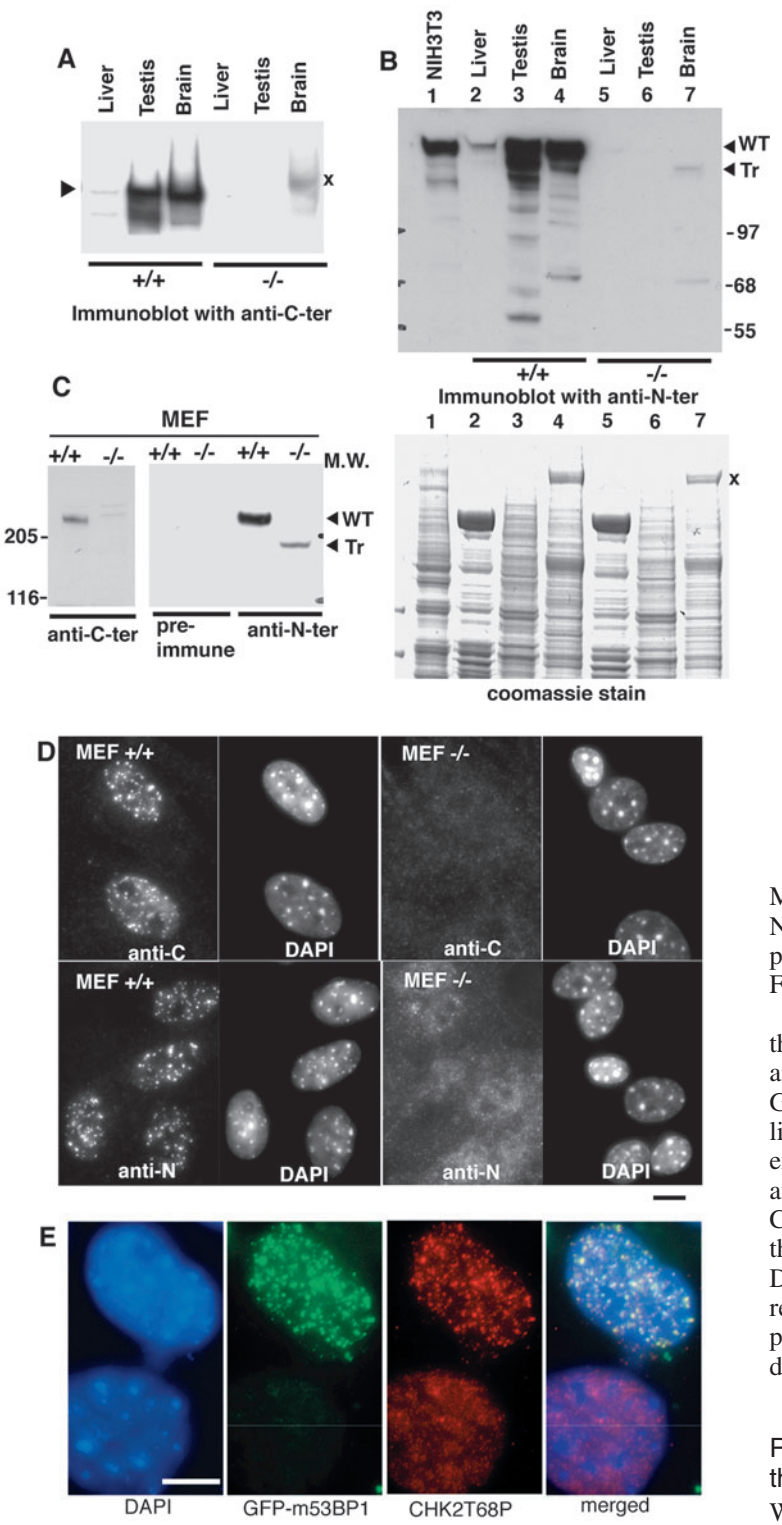

Fig. 2. GFP-m53BP1 complements a defect of cells lacking 53BP1. (A,B) Homozygous mutant mice that lack 10 exons of the 53BP1 gene, encoding the last 702 amino acids, were produced (see supplementary material Fig. S1). Western blot analysis of liver, testis and brain extracts from wild-type (+/+) and the mutant (–/–) mice with affinity-purified anti-C-terminus 53BP1 (residues 1255-1957) antibodies (A) or with anti-N-terminus (residues 1-355) antibodies (B). Each well was loaded with 25 μg of the total extracts indicated. The extracts from the mutant mice lack proteins recognized by the antibodies. In A, a faint smear in the –/– brain lane (marked by x) is non-specific binding to a highly expressed protein in the brain that corresponds to the protein band (marked by x) in B, lower panel. (C) Similar analysis was performed in MEF cells. Truncated 53BP1 (Tr) is detected in the total extracts of MEF cells from the mutant mice, when anti-N-terminus serum is used. The amount of the truncated protein is significantly lower than the wild-type protein (WT). Pre-immune serum for the anti-N-terminus did not react with any proteins. (D) MEF cells were exposed to 10 Gy of X rays, allowed to recover for 1 hour, fixed and subjected to staining with the antibodies indicated. In contrast to the wild-type 53BP1, which shows focal distribution, the truncated 53BP1 in mutant MEFs (–/–) does not show focal distribution when probed with anti-N antibodies. DNA was counterstained with DAPI. (E) GFP-m53BP1 fusion protein (green) was transiently expressed in the mutant MEF (–/–), irradiated with 10 Gy X rays, fixed and stained with anti-phospho-Chk2 antibodies (Chk2T68P; Cy3 in red). Bar, 10 μm.

smaller amount of the truncated protein in brain and MEF cells derived from the mutant mice (Fig. 2B, lane 7, 2C, right panel, –/–, anti-N-ter). Interestingly, the expression level of 53BP1 appears to be significantly higher in testis and brain than in liver in the wild-type animal (Fig. 2A,B, +/+). The truncated protein was not functional, since it was not concentrated in the nucleus and it failed to form nuclear foci after IR (Fig. 2D, MEF–/–, anti-N). Note that the preimmune serum for anti-N terminus antibodies showed little reaction with mouse proteins (Fig. 2C right panel; see supplementary material Fig. S1C for immunostaining).

Expression of GFP-m53BP1 in MEF cells derived from the mutant mice restored the IR-induced foci revealed by anti-Chk2T68P (Fig. 2E; compare the upper nucleus with GFP-m53BP1 and the lower without GFP-m53BP1). It is likely that the anti-Chk2T68P antibodies used in this experiment recognize other proteins phosphorylated after DNA damage induction as well as phosphorylated Chk2; therefore, the foci do not necessarily represent the accumulation of phosphorylated Chk2 at the DNA damage sites (Lukas et al., 2003). However, the result indicated that GFP-m53BP1 facilitated the phosphorylation of the protein(s) in the proximity of DNA damage.

Reduced mobility of 53BP1 after association with the sites of DNA damage

We examined the mobility of 53BP1 before and after IR using fluorescence recovery after photobleaching (FRAP) of the HeLa cells stably expressing GFP-m53BP1. In untreated cells, GFP-m53BP1 was distributed homogeneously over the chromatin. After bleaching a diffraction-limited spot in the nucleus of the untreated cells, the fluorescence of GFP-m53BP1 recovered rapidly to about 90% of the original level before photobleaching (Fig. 3A,B). The mobile fraction was 96.6%±1.5% and time required for half-recovery ($t_{½}$) was 2.37±0.59 seconds. GFP, localized to the nucleus, was

completely mobile and had $t_{1/2}$ of 0.32±0.08 seconds under the same experimental conditions (Fig. 3C).

Next, we used FRAP to analyse the IRIF-associated GFP-m53BP1. The HeLa cells stably expressing GFP-m53BP1 were exposed to 10 Gy of X rays and incubated for 1 hour to allow assembly of 53BP1 foci before FRAP assays. We used a lower power setting of the pulse laser that did not induce DNA damage but was strong enough for photobleaching. The FRAP profile of GFP-m53BP1 was considerably different after association with IRIF (Fig. 3D,E; see also Movie 2 in supplementary material). The fluorescence intensity curve was plotted using the mean of eight IRIF, each in a different nucleus from eight different experiments. First, the fluorescence recovery of GFP-m53BP1 was much slower at IRIF than homogenously distributed GFP-m53BP1 in untreated cells. Second, the final extent of recovery varied significantly among the foci (60-120%). This is manifested by the relatively large standard deviation towards the end of the curve. However, the recovery rate was similar between foci at the early stages of recovery. The plot gives $t_{1/2}$ of 318 seconds, which is more than 100 times slower than that of untreated cells. In six foci out of eight, the intensities reached a plateau (60-80%) in 800 to 1000 seconds. In the other foci, the recovery slowed down around the same time; however, the intensity continued to increase at a slower rate and exceeded 100%. At 1 hour after IR, the fluorescence intensity of some 53BP1 foci did not reach a plateau, and the foci continued to increase in size and fluorescence intensity (data not shown). This phenomenon might contribute to the slow increase of fluorescence intensities observed in the latter cases. The foci that showed a final recovery of 60-80% of the original intensities had an immobile fraction of GFP-m53BP1 that remained in the IRIF for at least 30 minutes. This suggests some heterogeneity of 53BP1 activity at chromatin in the proximity of DNA damage.

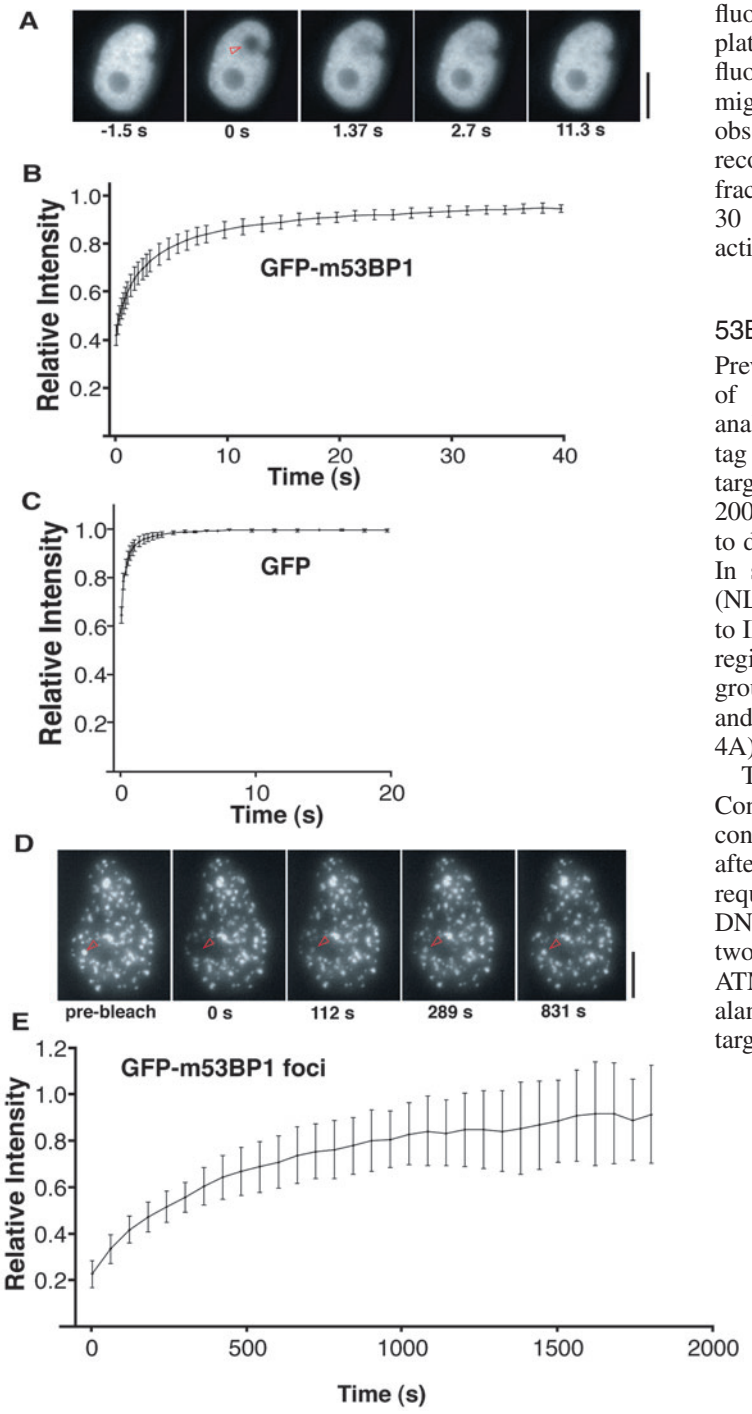

53BP1 foci targeting domain

Previously we mapped the kinetochore-binding domain (KBD) of mouse 53BP1 to residues 1220-1601 by GFP-fusion analysis (Jullien et al., 2002). Similar strategies using the HA-tag have been applied to identify the domain required for targeting 53BP1 to IRIF (Iwabuchi et al., 2003; Morales et al., 2003; Ward et al., 2003a). We used the GFP-fusion constructs to determine the minimal domain required for focal targeting. In summary, the KBD plus the nuclear localization signal (NLS, mapped to 1645-1703) was sufficient for the targeting to IRIF (Fig. 4C,D). Hereafter, we call this minimum essential region (1220-1703) the M domain. The data published by other groups were mostly consistent with ours, except for one point, and we describe our results briefly below (summarized in Fig. 4A).

The BRCT motifs are outside the M domain (Fig. 4A, 'M'). Constructs (GFP-NLS-BRCT and GFP-Δ2-BRCT) that contain the BRCT tandem repeats failed to assemble into foci after IR (Fig. 4E,F). Therefore, the BRCT motifs are neither required nor sufficient for 53BP1 foci assembly at the sites of DNA damage (Iwabuchi et al., 2003). The M domain contains two SQ motifs that are putative phosphorylation sites for the ATM-related kinases. Replacement of the serine residues with alanine at the two SQ motifs in the M domain did not abolish targeting activity (data not shown). These results are consistent

Fig. 3. FRAP analysis of GFP-m53BP1. (A) Fluorescence recovery kinetics of GFP-m53BP1 in non-irradiated HeLa cells. Images before bleaching (–1.5 s), immediately after the photobleach event (0 s), and later in the time course. The photobleached region is indicated by an arrowhead. (B) Relative intensities are plotted versus time in seconds (n=10). (C) FRAP analysis of GFP-NLS serves as a control (n=12). (D) Photobleaching and recovery of GFP-m53BP1 focus (indicated by an arrowhead) induced by exposure to 10 Gy of X rays. (E) Relative intensities of the GFP-m53BP1 foci plotted versus time after photobleaching (n=8). Values represent means±s.d. Bars, 10 μm.

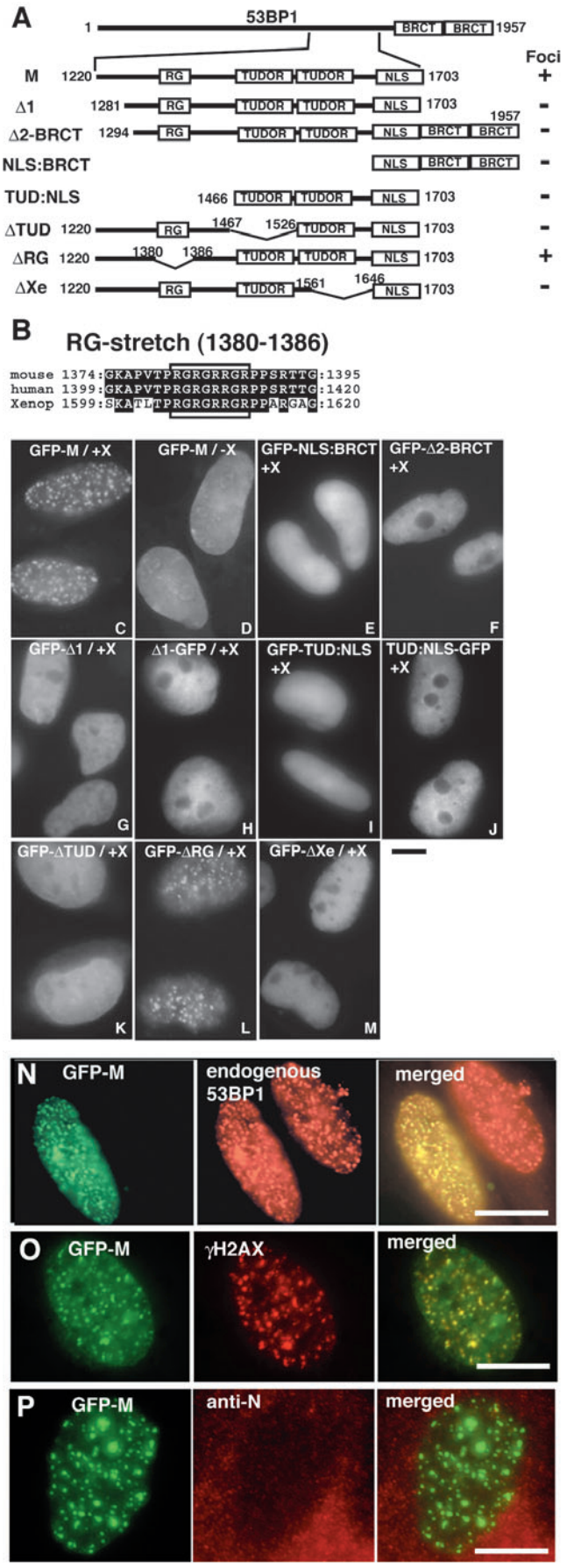

with published data (Iwabuchi et al., 2003; Morales et al., 2003; Ward et al., 2003a).

Further deletion of the M domain (Fig. 4A; Δ1, Δ2-BRCT, TUD-NLS) led to the loss of foci targeting (Fig. 4F-J). The images shown in Fig. 4 were taken at 1 or 2 hours after IR. The same results were obtained at 4 hours post-IR (data not shown). This is inconsistent with the data published by another group (Iwabuchi et al., 2003), who showed that a smaller domain of human 53BP1 (1480-1616, corresponding to our TUD-NLS construct) was sufficient for the targeting to IRIF.

We verified the expression of the fusion proteins at their predicted size by western blotting using anti-GFP antibodies (supplementary materials Fig. S1F and data not shown). Addition of the GFP moiety at the N-terminus of the 53BP1 sub-domains might disturb their targeting. Thus, we made constructs expressing GFP fused to the C-terminus of Δ1 (1281-1703) and TUD-NLS (1466-1703). Neither Δ1-GFP nor TUD-NLS-GFP was able to target to the IRIF (Fig. 4H,J).

As shown in Fig. 1D, the accumulation of the GFP-M to the sites of DNA damage was slower than that of full-length GFP-m53BP1. In addition, the intensity of the GFP-M stripe was significantly dimmer than that of GFP-m53BP1 and often difficult to discern at early stages. Therefore the minimum domain for the targeting of the GFP-fusion to IRIF is located in residues 1220-1703; however, the domain is not sufficient for targeting as rapidly as the full-length m53BP1.

The M domain contains a tandem repeat of Tudor motifs spanning residues 1469-1520 and 1523-1574 (Altschul et al., 1997; Charier et al., 2004; Huyen et al., 2004; Sanders et al., 2004). It has been noted that the domain is weakly conserved in the yeast Crb2 and Rad9 proteins (Huyen et al., 2004). The Tudor motif has been found in a number of proteins involved in RNA metabolic processes (Ponting, 1997). The M domain also contains an arginine- and glycine-rich (RG) stretch, which is found in some RNA processing factors (Fig. 4B). The GFP-M fusion lacking the Tudor motif (GFP-ΔTUD) did not target to the damage-induced foci (Fig. 4K) (Iwabuchi et al., 2003). Deletion of the RG-stretch did not abolish the foci targeting in HeLa cells, although we observed some reduction of its targeting efficiency in MEF cells lacking endogenous 53BP1 (Fig. 4L; see below). We noticed that residues 1561-1646 of mouse 53BP1 are not conserved in our cDNA clone of the *Xenopus* homologue (supplementary material Fig. S1E). Deletion of this region leads to loss of the foci-targeting

Fig. 4. Essential domain of 53BP1 for targeting to the nuclear foci induced by IR. (A) Schematic diagram of GFP-fusion constructs. The various portions of mouse 53BP1 were fused at their N-terminus (in some cases at their C-terminus) to GFP and tested for their ability to target (+) or not (–) to the IR-induced 53BP1 foci. The positions of the RG stretch (RG), Tudor motifs, nuclear localization signal (NLS) and BRCT motifs are boxed. (B) Amino acid sequence alignment of the RG-stretch in mouse, human and *Xenopus* 53BP1. (C-M) HeLa cells were transfected with the GFP-fusion constructs indicated, treated with (+) or without (–) irradiation of 10 Gy X rays and observed under a fluorescent microscope. (N) Endogenous 53BP1 was visualized with an antibody to the N-terminus of 53BP1 (red) that does not recognize the M (minimum) domain, in NIH3T3 cells expressing GFP-M (green). (O,P) GFP-M fusion protein (green) was transiently expressed in the mutant MEF (–/–), irradiated with 10 Gy X rays, fixed, and stained with anti-γH2AX antibodies (Cy3 in red) or with anti-N-terminus m53BP1 (Cy3 in red). Bars, 10 μm.

activity (Fig. 4M, GFP-ΔXe). This was unexpected, since GFP fused to the *Xenopus* 53BP1 can target to IRIF (data not shown). This domain (1561-1646) overlaps with the second Tudor motif.

The targeting of GFP-M does not require endogenous 53BP1

We confirmed that the GFP-M fusion protein co-localises with endogenous 53BP1 by immunostaining with antibodies to the N-terminal 355 residues of m53BP1 (Fig. 4N). However, GFP-M was not recruited to the damage-induced foci through a possible interaction of the M domain with the endogenous 53BP1. In the MEF$^{-/-}$ cells, the GFP-M protein forms foci 1 hour after IR that co-localise exactly with the γH2AX foci (Fig. 4O, GFP-M). The mutant MEF cells express truncated 53BP1, which is recognized by antibodies against the N-terminus of m53BP1. However, the truncated protein did not associate with foci formed by GFP-M (Fig. 4P). We conclude that the M domain of 53BP1 has the ability to target to damage-induced foci independently, although the targeting kinetics was slower as shown in Fig. 1D.

Although deletion of the RG-stretch did not abolish foci targeting, the targeting of GFP-ΔRG might be assisted by endogenous 53BP1 in HeLa cells. We examined the targeting efficiency of GFP-ΔRG in the mutant MEFs. In the mutant MEF cells that lack functional 53BP1, GFP-ΔRG localised at the IRIF, although with a significantly lower efficiency (48%) compared with that of GFP-M (90%) (Table 1). Even in wild-type MEF cells, the targeting efficiency of GFP-ΔRG was slightly lower (68%) than that of GFP-M (88%). Thus the RG-stretch facilitates the foci targeting, although it is not absolutely essential.

Dissociation of 53BP1 from the IR-induced foci by RNase treatment

The presence of the Tudor motif and the RG-stretch in the M domain suggested a possible involvement of RNA in 53BP1 foci assembly. We examined whether the association of 53BP1 at IRIF was sensitive to ribonuclease treatment (Maison et al., 2002). NIH3T3 cells were permeabilised with detergent (0.5% Tween 20) after IR and incubated with or without RNase A (1 mg/ml); 53BP1 was visualized by immunostaining (Fig. 5A,B). The cells treated with RNase A/Tween 20 showed significant dissociation of 53BP1 from the foci compared with those treated with Tween 20 alone (Fig. 5, compare panels A and B). A different fixation procedure (paraformaldehyde) gave similar results (data not shown). Western blot analysis confirmed that this dissociation was not due to degradation of the protein (Fig. 5C). 53BP1 foci were not dissociated by treatment with RNase H, which specifically acts on RNA/DNA or RNA/RNA duplexes (Fig. 5D). The RNase A-treatment does not show any effect on the phosphorylated H2AX foci, which occur prior to the recruitment of 53BP1 (Fig. 5E,F).

In HeLa cells, 53BP1 dissociation by RNase A required a higher concentration of the detergent. Treatment with 2% Tween 20 and 1 mg/ml RNase A effectively dissociated 53BP1 from the IRIF (Fig. 5J). 53BP1 remained associated with IRIF after treatments with 0.5% Tween 20 alone (Fig. 5G), with 0.5% Tween 20 plus RNase A (Fig. 5H) or with 2% Tween 20 alone (Fig. 5I). This was not because permeabilisation of HeLa nuclei required a higher concentration of the detergent, since treatment with 0.5% Tween 20 plus DNase I effectively disassembled 53BP1 foci (data not shown). Treatment with 1 mg/ml RNase A plus 0.5% Triton X-100 did not dissociate 53BP1 from IRIF (Ward et al., 2003a) (our own observation). This variability between human and mouse cells suggests that there are several ways for 53BP1 to associate with the IRIF (e.g. through interaction with γ-H2AX or with DNA ends) (Iwabuchi et al., 2003; Ward et al., 2003a).

Table 1. Targeting efficiency of GFP-M and GFP-ΔRG in MEF cells derived from 53BP1-knockout mice

	+/+		–/–	
	0 Gy	10 Gy	0 Gy	10 Gy
GFP-M	0%	88%	8%	90%
GFP-ΔRG	0%	68%	4%	48%

Wild type MEF cells (+/+) or the 53BP1 mutant MEF cells (–/–) were transfected with the plasmids expressing GFP-M or GFP-ΔRG. The GFP signals were either focal or homogenous inside the nucleus. The percentage of cells with the focal distribution of the GFP-fusion protein are indicated. Fifty cells were scored in each case. The cells expressing an excess amount of the GFP-fusions were not scored to exclude artefactual effects. GFP-ΔRG is less efficient for the IRIF targeting.

The IR-induced foci of the GFP-M fusion were not dissociated by treatment with 0.5% Tween 20 plus RNase A in HeLa cells (Fig. 5L,P,W). We investigated whether deletion of the RG stretch had any impact on this RNase resistance in the presence of 0.5% Tween 20 in HeLa cells. HeLa cells were transfected either with GFP-M or with GFP-ΔRG, exposed to IR, permeabilised with 0.5% Tween 20 after 20 minutes, 1 hour or 2 hours and treated with RNaseA. We found that at earlier stages after IR, the focal association of GFP-ΔRG was significantly more sensitive to RNaseA treatment than that of GFP-M (Fig. 5, panels N, R versus L, P). The focal appearance of GFP-ΔRG was almost lost at 20 minutes (N) and diminished at 1 hour (R), respectively, although 0.5% Tween 20 alone made the foci less distinct at 20 minutes (M). Treatment with RNaseH did not have any effect (S). Strikingly, re-addition of nuclear RNA after RNaseA treatment of cells at 1 hour post-IR restored the focal association of GFP-ΔRG (Fig. 5, compare R and T). Re-addition of tRNA did not restore the GFP-ΔRG foci (U). Later, at 2 hours post-IR, GFP-ΔRG was not dissociated from IRIF by treatment with RNase A (Fig. 5Y). By contrast, the association of GFP-M did not show strong sensitivity to RNase A throughout the recovery period (Fig. 5L,P,W). Thus, in HeLa cells, deletion of the RG stretch unveiled a process where the tethering of the M domain to the IRIF was more sensitive to RNase A treatment. The results also suggested that an RNA component plays a role particularly in the earlier stages of 53BP1 foci formation in HeLa cells.

Co-immunoprecipitation of RNA with 53BP1

We examined the association of RNA with 53BP1 by immunoprecipitation followed by radiolabelling of RNA (Fig. 6). Either anti-53BP1 antibodies or normal rabbit IgG were added to HeLa nuclear extracts, followed by addition of protein A-Sepharose beads. The beads were washed with buffers containing 100 mM sodium acetate or 150 mM sodium

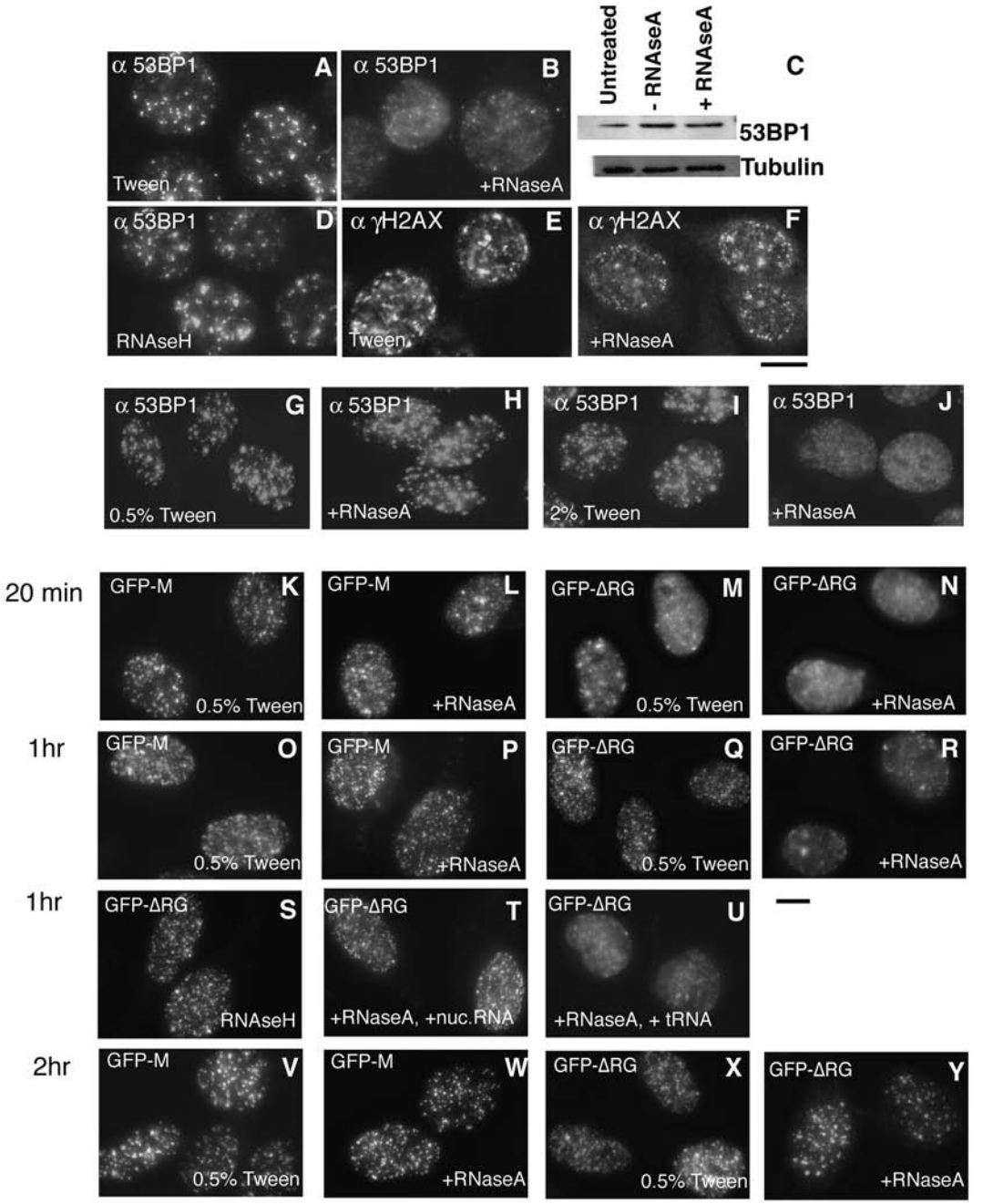

Fig. 5. RNase treatment dissociates 53BP1 from the damage-induced foci. (A,B) NIH3T3 cells exposed to X rays were permeabilised with 0.5% Tween 20, treated with (B) or without (A) 1 mg/ml RNase A, fixed, and stained for 53BP1. The level of 53BP1 associated with the foci reduces significantly after treatment with RNase A. (C) Western blot for the samples treated with or without RNase A shows that this reduction is not due to degradation of 53BP1. Equal amounts of total protein were loaded in each lane. The blots for tubulin confirm equal loading. (D) Treatment with an endoribonuclease for RNA/DNA duplexes (RNase H) does not dissociate 53BP1 from the foci. (E,F) In contrast to 53BP1, phosphorylated γ-H2AX foci are not affected by RNase treatment. (G,H) X-irradiated HeLa cells were treated either with 0.5% Tween 20 alone (G) or with 0.5% Tween 20 plus RNase A (H). In the presence of 2% Tween 20 (I,J), 53BP1 was dissociated specifically by RNase A treatment (J). (K-Y), HeLa cells were transfected with plasmids expressing the GFP-M domain fusion or GFP-ΔRG (M domain lacking the RG stretch). The cells were exposed to 10 Gy of X rays, incubated at 37°C for the period indicated (K-N, for 20 minutes; O-U, for 1 hour; V-Y, for 2 hours) and permeabilised with Tween 20. Cells were treated with (L,N,P,R,T,U,W,Y) or without (K,M,O,Q,V,X) RNase A after permeabilisation. (S) Cells were treated with RNase H. (T,U) After RNase A treatment, cells were treated with RNase inhibitor and then incubated with nuclear RNA (T) or with tRNA (U). Bars, 10 μm.

chloride. Nucleic acids were extracted from the beads. The extracted RNA was end-labeled with [5′-^{32}P]pCp and RNA ligase, separated on a denaturing polyacrylamide gel and autoradiographed.

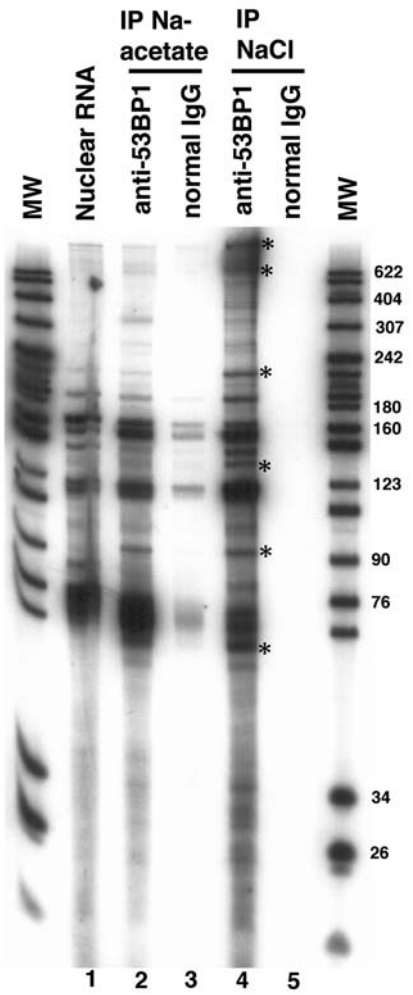

Fig. 6. Association of 53BP1 with RNA. RNA was extracted from 53BP1 immunoprecipitates (lanes 2 and 4) and from normal rabbit IgG control (lanes 3 and 5), labelled with [^{32}P]pCp, separated on a 6% denaturing polyacrylamide gel, and auto-radiographed. Total nuclear RNA was labelled and used as a control (lane1). After incubation with HeLa nuclear extracts, immuno-affinity beads were washed in two different buffers. In one set (lanes 2 and 3), 100 mM sodium acetate was used as a salt. In the other set (lanes 4 and 5), 150 mM sodium chloride was used. Several bands were enriched in the 53BP1 precipitates (marked with asterisks). Molecular weight marker (MW) was end-labelled fragments of pBR322 digested with *Msp*I. Sizes are indicated as nucleotide length.

A number of RNA molecules co-immunoprecipitated with 53BP1 (Fig. 6, lanes 2,4). In the presence of 150 mM NaCl, the RNA association with the immunoprecipitates was anti-53BP1 antibody specific and little RNA was detected in the precipitates with control IgG (Fig. 6, lanes 4,5). Several bands were clearly enriched in the 53BP1 immunoprecipitates (marked with asterisks) if the lane was compared with that of total nuclear RNA (Fig. 6, lane 1). We have cloned the cDNA from some of the major bands in a larger scale 53BP1 immunoprecipitation and identified U1 (165 nucleotides), U2 (185 nucleotides), MRP (265 nucleotides) and 7SL (305 nucleotides) RNA (Y.A., unpublished). The interaction between 53BP1 and RNA provided further support for the potential involvement of RNA in 53BP1 foci assembly. However, the spectrum of RNA co-precipitating with 53BP1 was broad (rather non specific) and it is unknown whether a specific RNA functions as a tether of 53BP1 to the IRIF or whether the general affinity of 53BP1 complex to RNA is important for its function.

Discussion

The cellular response to DNA damage is rapid. If cells are exposed to IR, ATM kinase is instantly activated and phosphorylates histone subtype H2AX near the sites of DNA damage, which subsequently leads to the formation of ionizing radiation-induced foci (IRIF). Although the functional significance of IRIF assembly is not well understood at the moment, IRIF may facilitate repair of the damaged DNA and activation of the appropriate checkpoint signal transduction pathway (Bradbury and Jackson, 2003). In the present study, we have investigated the dynamics of GFP-m53BP1 using live cell imaging. We observed that GFP-m53BP1 starts to accumulate at the sites of DNA damage 2 minutes after irradiation. FRAP analysis showed that GFP-m53BP1 is mobile in non-irradiated cells ($t_{½}$=2.37 seconds). GFP (29 kDa) is thought to move relatively freely in the nucleus, and this is confirmed by our results ($t_{½}$ was 0.32 seconds). The calculated molecular weight of 53BP1 is 211 kDa and the protein was eluted as a 1 MD complex from a gel filtration column (Anderson et al., 2001). Given the fact that the diffusion coefficient is proportional to the inverse of the cube root of the molecular mass (Reits and Neefjes, 2001), the $t_{½}$ of 53BP1 appears to be larger than expected from its size and nearly equivalent to that of GFP-HP1, a heterochromatin-binding protein (Cheutin et al., 2003). We hypothesise that 53BP1 does not diffuse freely in the inter-chromatin space. The protein may have some affinity for chromatin in untreated cells, repeatedly binding to and dissociating from chromatin, which might facilitate surveillance of DNA integrity and the rapid recruitment of 53BP1 to the sites of damage. After association with IRIF, the exchange rate of GFP-53BP1 becomes significantly slower ($t_{½}$=318 seconds). This slow recovery rate of 53BP1 at IRIF appears to be lower than those of histone H1 ($t_{½}$=18.7 seconds) (Lever et al., 2000) and Rad52 at IRIF ($t_{½}$=26 seconds) (Essers et al., 2002). Rad51, a recA homologue of eukaryotes, shows little exchange once it binds to the sites of DNA damage (Essers et al., 2002). By contrast, Nbs1, which forms a complex with Rad50 and Mre11, appears to exchange more rapidly even after association with IRIF ($t_{½}$ is several seconds) (Lukas et al., 2003). The greatly reduced mobility of 53BP1 at IRIF indicates that the chromatin near the DNA damage should have a significantly higher affinity for 53BP1, and it would be interesting to investigate the underlying molecular mechanisms.

To understand the mechanism of assembly at IRIF, it was important to determine the domain of 53BP1 essential for focal targeting. The minimum (M) domain of 53BP1, which is necessary and sufficient for assembly at the sites of DNA damage, consists of residues 1220-1703. Several reports have been published for the targeting domain analysis of 53BP1, and they were mostly consistent with ours except for one point (Iwabuchi et al., 2003; Morales et al., 2003; Ward et al., 2003a). Iwabuchi et al. found that the region (1480-1616)

encompassing the Tudor to NLS region of human 53BP1 was sufficient for IRIF targeting (the domain was fused with an HA-tag) (Iwabuchi et al., 2003). All of our constructs failed to target to the IRIF if they had further N-terminus deletions, although they included the corresponding mouse domain. They were GFP-Δ1(1281-1703), Δ1(1281-1703)-GFP, GFP-Δ2-BRCT(1294-1957), GFP-TUD-NLS(1466-1703), and TUD-NLS(1466-1703)-GFP. The reasons for this discrepancy remain unclear. The use of different tags might offer a possible explanation (GFP in this study and HA-tag in the others). Alternatively, it may reflect a difference between human and mouse 53BP1. Ward et al. showed that residues 956-1354 of human 53BP1 interact directly with γH2AX in vitro (Ward et al., 2003a). Note that this domain is outside the minimum-targeting domain identified by Iwabuchi et al. Our results with living cells showed that the appearance of GFP-M at the laser-induced DNA damage sites was significantly slower than that of GFP-m53BP1. This indicated that residues outside the M domain appear to increase the rate of 53BP1 accumulation at IRIF.

The M domain contains an RG stretch and two Tudor motifs, found in a number of proteins implicated in RNA metabolism (Paushkin et al., 2002; Ponting, 1997). The Tudor motifs of 53BP1 are essential for the focal targeting, and the presence of the RG-stretch increases the targeting efficiency. These observations prompted us to examine the possible involvement of RNA in the targeting of 53BP1 to IRIF.

We have shown that treatment with RNase A but not RNase H leads to significant dissociation of 53BP1 from the IRIF in NIH3T3 and HeLa cells (Fig. 5). This suggests that an RNA component is required to tether 53BP1 at the sites of DNA damage. The inability of RNase H to dissociate 53BP1 from IRIF indicates that the RNA involved in tethering 53BP1 is unlikely to be directly complementary or binding to the damaged DNA. In HeLa cells, the association of 53BP1 to IRIF is more resistant to RNase A and it requires the presence of a higher concentration of Tween 20 for the dissociation of 53BP1 from IRIF. Since the entire 53BP1 protein is highly conserved in sequence between the mouse and human, we speculate that this variation is more likely due to other proteins involved in IRIF assembly. In HeLa cells, the association becomes sensitive specifically at earlier stages of the post-IR period if the protein lacks its RG stretch (Fig. 5). It is likely that RNA is but one of many components that tether 53BP1 to IRIF, and plays a more critical role at the early stages of 53BP1 foci assembly in HeLa cells. It is possible that the RNA component is necessary only in the assembly process of 53BP1 foci and, once the association is established, it is not be required for their maintenance.

53BP1 is associated with a large protein complex (Anderson et al., 2001). Immunoprecipitates with anti-53BP1 antibodies contain some RNA and several protein components of RNPs (this study; and J. Strafford and Y.A., unpublished). Although the specificity and significance of these interactions require further investigation, the observation is consistent with the possible involvement of RNA in 53BP1 focus formation. It is noteworthy that there are several reports showing association of U2 snRNA with proteins involved in DNA damage repair as well as splicing factors (Brand et al., 2001; Caspary et al., 1999; Martinez et al., 2001). MRP RNA is a component of the RNase MRP complex and mutations of MRP RNA cause a pleiotropic genetic disorder, Carilage-Hair Hypoplasia (CHH) (Ridanpaa et al., 2001). Part of the CHH phenotypes is predisposition to several cancers.

Association of HP1α to pericentric heterochromatin depends on its chromodomain, which binds to histone H3 methylated at lysine 9, and also on an RNA-binding activity present in the hinge region of the protein (Maison et al., 2002; Muchardt et al., 2002). The Tudor motif of the SMN protein binds to a symmetrically methylated RG-stretch of the Sm proteins of splicing snRNPs (Sprangers et al., 2003). The 3D structure of the Tudor domain (a three β-stranded core) is similar to that of the chromo domain, and recently it has been shown that the Tudor motifs of human 53BP1 bind histone H3 methylated at lysine 79 (H3-K79) (Huyen et al., 2004; Maurer-Stroh et al., 2003). However, the H3-K79 is constitutively methylated and it is more likely that its accessibility to 53BP1 changes in response to DNA damage (Huyen et al., 2004; Sanders et al., 2004). An RNA component might be involved in this exposing process by altering the local chromatin structure. It was also shown that the Tudor domain of 53BP1 is involved in binding to the 53BP1 RG-stretch and to DNA (Charier et al., 2004). Our recent experiments indicate that 53BP1 itself is methylated in vivo (Y.A., unpublished). This suggests an intramolecular interaction between the Tudor motifs and the RG-stretch or intermolecular interactions between 53BP1 molecules themselves.

We previously showed that the same M domain is sufficient for the targeting of 53BP1 to the kinetochore during mitosis (Jullien et al., 2002). However, it is unlikely that the kinetochore localization of 53BP1 is due to DNA lesions on the centromere DNA. First, 53BP1 localizes at the fibrous corona of kinetochores, which does not contain detectable DNA (Cooke et al., 1990; Cooke et al., 1997; Jullien et al., 2002). Second, in interphase cells, 53BP1 does not co-localize with kinetochores (Jullien et al., 2002). Third, anti-γH2AX antibody does not stain the kinetochores of mitotic chromosomes (Rogakou et al., 1999) (data not shown). Fourth, 53BP1 is detected on kinetochores of mitotic chromosomes in H2AX-deficient cells (Ward et al., 2003a). The fact that the same M domain targets kinetochores and IRIF suggests that targeting to kinetochore and targeting to IRIF share a common mechanism, although they are initiated by different checkpoint signals. It is interesting that the targeting of HP1 to the centromeric heterochromatin and the targeting of 53BP1 to IRIF appear to involve similar components: RNA and structurally homologous motifs (chromodomain of HP1 and Tudor domain of 53BP1). In fission yeast, centromeric heterochromatic silencing and histone H3 methylation is regulated by RNA interference, possibly involving double-stranded RNA arising from centromeric repeats (Volpe et al., 2002). Kinetochore binding of 53BP1 might involve some of these molecular signals on the condensed heterochromatin. However, it is worth noting that ES cells lacking functional 53BP1 do not show a significant increase in aneuploidy (D.J., unpublished), suggesting that the protein is unlikely to be a critical component of mitotic spindle checkpoint control.

Our results demonstrate a functional link between RNA and the DNA damage response. Another vertebrate BRCT protein, BRCA1, associates with Xist RNA and is involved in the inactive X chromosome structure (Ganesan et al., 2002). Recruitment of 53BP1 to the sites of DNA damage might

require a close interaction of the 53BP1 complex with on-going RNA metabolism occurring on chromatin (e.g. interaction with RNA processing machineries). Recently Kao et al. identified histone deacetylase HDAC4 as an IRIF-associated protein, and showed that HDAC4 co-immunoprecipitates with 53BP1 (Kao et al., 2003). 53BP1 may play a role in DNA-damage-induced chromatin-modification as well as providing an assembly platform for proteins involved in repair and DNA-damage-checkpoint signal transduction (Fernandez-Capetillo et al., 2002; Wang et al., 2002). The mice lacking functional 53BP1 show defects in the immunoglobulin class-switch recombination (Manis et al., 2004).

The results of our experiments may provide fresh insight into the complex intranuclear mechanism mediating the cellular response to DNA damage by IR.

We thank C. Morrow, L. Anderson, M. Brewis, A. Roberts and J. Strafford for preliminary results and experimental support; K. Samejima, W. C. Earnshaw, A. Bird and J. Swedlow (University of Dundee) for advice and discussions; and K. Hardwick, R. Allshire, T. Toda and S. MacNeill for their comments on the manuscript. We thank S. Swift for assistance with FRAP experiments performed at the Wellcome Trust Biocentre Light Microscopy Facililty, Dundee, Scotland. Y.A. was supported by the Wellcome Trust. D.W.M. was supported by a programme grant (SP2095/0301) from Cancer Research UK.

References

Altschul, S. F., Madden, T. L., Schaffer, A. A., Zhang, J., Zhang, Z., Miller, W. and Lipman, D. J. (1997). Gapped BLAST and PSI-BLAST: a new generation of protein database search programs. *Nucleic Acids Res.* **25**, 3389-3402.

Anderson, L., Henderson, C. and Adachi, Y. (2001). Phosphorylation and rapid relocalization of 53BP1 to nuclear foci upon DNA damage. *Mol. Cell. Biol.* **21**, 1719-1729.

Andrews, P. D., Ovechkina, Y., Morrice, N., Wagenbach, M., Duncan, K., Wordeman, L. and Swedlow, J. R. (2004). Aurora B regulates MCAK at the mitotic centromere. *Dev. Cell* **6**, 253-268.

Axelrod, D., Koppel, D. E., Schlessinger, J., Elson, E. and Webb, W. W. (1976). Mobility measurement by analysis of fluorescence photobleaching recovery kinetics. *Biophys. J.* **16**, 1055-1069.

Bassing, C. H., Chua, K. F., Sekiguchi, J., Suh, H., Whitlow, S. R., Fleming, J. C., Monroe, B. C., Ciccone, D. N., Yan, C., Vlasakova, K. et al. (2002). Increased ionizing radiation sensitivity and genomic instability in the absence of histone H2AX. *Proc. Natl. Acad. Sci. USA* **99**, 8173-8178.

Bork, P., Hofmann, K., Bucher, P., Neuwald, A. F., Altschul, S. F. and Koonin, E. V. (1997). A superfamily of conserved domains in DNA damage-responsive cell cycle checkpoint proteins. *FASEB J.* **11**, 68-76.

Bradbury, J. M. and Jackson, S. P. (2003). The complex matter of DNA double-strand break detection. *Biochem. Soc. Trans.* **31**, 40-44.

Brand, M., Moggs, J. G., Oulad-Abdelghani, M., Lejeune, F., Dilworth, F. J., Stevenin, J., Almouzni, G. and Tora, L. (2001). UV-damaged DNA-binding protein in the TFTC complex links DNA damage recognition to nucleosome acetylation. *EMBO J.* **20**, 3187-3196.

Caspary, F., Shevchenko, A., Wilm, M. and Seraphin, B. (1999). Partial purification of the yeast U2 snRNP reveals a novel yeast pre-mRNA splicing factor required for pre-spliceosome assembly. *EMBO J.* **18**, 3463-3474.

Celeste, A., Petersen, S., Romanienko, P. J., Fernandez-Capetillo, O., Chen, H. T., Sedelnikova, O. A., Reina-San-Martin, B., Coppola, V., Meffre, E., Difilippantonio, M. J. et al. (2002). Genomic instability in mice lacking histone H2AX. *Science* **296**, 922-927.

Celeste, A., Fernandez-Capetillo, O., Kruhlak, M. J., Pilch, D. R., Staudt, D. W., Lee, A., Bonner, R. F., Bonner, W. M. and Nussenzweig, A. (2003). Histone H2AX phosphorylation is dispensable for the initial recognition of DNA breaks. *Nat. Cell. Biol.* **5**, 675-679.

Charier, G., Couprie, J., Alpha-Bazin, B., Meyer, V., Quemeneur, E., Guerois, R., Callebaut, I., Gilquin, B. and Zinn-Justin, S. (2004). The Tudor tandem of 53BP1: a new structural motif involved in DNA and RG-rich peptide binding. *Structure* **12**, 1551-1562.

Cheutin, T., McNairn, A. J., Jenuwein, T., Gilbert, D. M., Singh, P. B. and Misteli, T. (2003). Maintenance of stable heterochromatin domains by dynamic HP1 binding. *Science* **299**, 721-725.

Cooke, C. A., Bernat, R. L. and Earnshaw, W. C. (1990). CENP-B: a major human centromere protein located beneath the kinetochore. *J. Cell Biol.* **110**, 1475-1488.

Cooke, C. A., Schaar, B., Yen, T. J. and Earnshaw, W. C. (1997). Localization of CENP-E in the fibrous corona and outer plate of mammalian kinetochores from prometaphase through anaphase. *Chromosoma* **106**, 446-455.

Derbyshire, D. J., Basu, B. P., Serpell, L. C., Joo, W. S., Date, T., Iwabuchi, K. and Doherty, A. J. (2002). Crystal structure of human 53BP1 BRCT domains bound to p53 tumour suppressor. *EMBO J.* **21**, 3863-3872.

Dignam, J. D., Lebovitz, R. M. and Roeder, R. G. (1983). Accurate transcription initiation by RNA polymerase II in a soluble extract from isolated mammalian nuclei. *Nucleic Acids Res.* **11**, 1475-1489.

DiTullio, R. A., Jr, Mochan, T. A., Venere, M., Bartkova, J., Sehested, M., Bartek, J. and Halazonetis, T. D. (2002). 53BP1 functions in an ATM-dependent checkpoint pathway that is constitutively activated in human cancer. *Nat. Cell Biol.* **4**, 998-1002.

Du, L. L., Nakamura, T. M., Moser, B. A. and Russell, P. (2003). Retention but not recruitment of Crb2 at double-strand breaks requires Rad1 and Rad3 complexes. *Mol. Cell. Biol.* **23**, 6150-6158.

Dulic, A., Bates, P. A., Zhang, X., Martin, S. R., Freemont, P. S., Lindahl, T. and Barnes, D. E. (2001). BRCT domain interactions in the heterodimeric DNA repair protein XRCC1-DNA ligase III. *Biochemistry* **40**, 5906-5913.

Essers, J., Houtsmuller, A. B., van Veelen, L., Paulusma, C., Nigg, A. L., Pastink, A., Vermeulen, W., Hoeijmakers, J. H. and Kanaar, R. (2002). Nuclear dynamics of RAD52 group homologous recombination proteins in response to DNA damage. *EMBO J.* **21**, 2030-2037.

Fernandez-Capetillo, O., Chen, H. T., Celeste, A., Ward, I., Romanienko, P. J., Morales, J. C., Naka, K., Xia, Z., Camerini-Otero, R. D., Motoyama, N. et al. (2002). DNA damage-induced G2-M checkpoint activation by histone H2AX and 53BP1. *Nat. Cell Biol.* **4**, 993-997.

Ganesan, S., Silver, D. P., Greenberg, R. A., Avni, D., Drapkin, R., Miron, A., Mok, S. C., Randrianarison, V., Brodie, S., Salstrom, J. et al. (2002). BRCA1 supports XIST RNA concentration on the inactive X chromosome. *Cell* **111**, 393-405.

Gilbert, C. S., Green, C. M. and Lowndes, N. F. (2001). Budding yeast Rad9 is an ATP-dependent Rad53 activating machine. *Mol. Cell* **8**, 129-136.

Grawunder, U., Zimmer, D. and Leiber, M. R. (1998). DNA ligase IV binds to XRCC4 via a motif located between rather than within its BRCT domains. *Curr. Biol.* **8**, 873-876.

Huyen, Y., Zgheib, O., Ditullio, R. A., Jr, Gorgoulis, V. G., Zacharatos, P., Petty, T. J., Sheston, E. A., Mellert, H. S., Stavridi, E. S. and Halazonetis, T. D. (2004). Methylated lysine 79 of histone H3 targets 53BP1 to DNA double-strand breaks. *Nature* **432**, 406-411.

Iwabuchi, K., Bartel, P. L., Li, B., Marraccino, R. and Fields, S. (1994). Two cellular proteins that bind to wild-type but not mutant p53. *Proc. Natl. Acad. Sci. USA* **91**, 6098-6102.

Iwabuchi, K., Basu, B. P., Kysela, B., Kurihara, T., Shibata, M., Guan, D., Cao, Y., Hamada, T., Imamura, K., Jeggo, P. A. et al. (2003). Potential role for 53BP1 in DNA end-joining repair through direct interacation with DNA. *J. Biol. Chem.* **278**, 36487-36495.

Joo, W. S., Jeffrey, P. D., Cantor, S. B., Finnin, M. S., Livingston, D. M. and Pavletich, N. P. (2002). Structure of the 53BP1 BRCT region bound to p53 and its comparison to the Brca1 BRCT structure. *Genes Dev.* **16**, 583-593.

Jullien, D., Vagnarelli, P., Earnshaw, W. C. and Adachi, Y. (2002). Kinetochore localisation of the DNA damage response component 53BP1 during mitosis. *J. Cell Sci.* **115**, 71-79.

Kao, G. D., McKenna, W. G., Guenther, M. G., Muschel, R. J., Lazar, M. A. and Yen, T. J. (2003). Histone deacetylase 4 interacts with 53BP1 to mediate the DNA damage response. *J. Cell Biol.* **160**, 1017-1027.

Keith, G. (1983). Optimization of conditions for labeling the 3′ OH end of tRNA using T4 RNA ligase. *Biochimie* **65**, 367-370.

Lever, M. A., Th'ng, J. P., Sun, X. and Hendzel, M. J. (2000). Rapid exchange of histone H1.1 on chromatin in living human cells. *Nature* **408**, 873-876.

Lewis, C. D., Lebkowski, J. S., Daly, A. K. and Laemmli, U. K. (1984). Interphase nuclear matrix and metaphase scaffolding structures. *J. Cell Sci. Suppl.* **1**, 103-122.

Li, J., Williams, B. L., Haire, L. F., Goldberg, M., Wilker, E., Durocher, D., Yaffe, M. B., Jackson, S. P. and Smerdon, S. J. (2002). Structural and functional versatility of the FHA domain in DNA-damage signaling by the tumor suppressor kinase Chk2. *Mol. Cell.* **9**, 1045-1054.

Limoli, C. L. and Ward, J. F. (1993). A new method for introducing double-strand breaks into cellular DNA. *Radiat. Res.* **134**, 160-169.

Lukas, C., Falck, J., Bartkova, J., Bartek, J. and Lukas, J. (2003). Distinct spatiotemporal dynamics of mammalian checkpoint regulators induced by DNA damage. *Nat. Cell Biol.* **5**, 255-260.

Maison, C., Bailly, D., Peters, A. H. F. M., Quivy, J.-P., Roche, D., Taddei, A., Lachner, M., Jenuwein, T. and Almouzni, G. (2002). Higher-order structure in pericentric heterochromatin involves a distinct pattern of histone modificatin and an RNA component. *Nat. Genet.* **30**, 329-334.

Manis, J. P., Morales, J. C., Xia, Z., Kutok, J. L., Alt, F. W. and Carpenter, P. B. (2004). 53BP1 links DNA damage-response pathways to immunoglobulin heavy chain class-switch recombination. *Nat. Immunol.* **5**, 481-487.

Manke, I. A., Lowery, D. M., Nguyen, A. and Yaffe, M. B. (2003). BRCT repeats as phosphopeptide-binding modules involved in protein targeting. *Science* **302**, 636-639.

Martinez, E., Palhan, V. B., Tjernberg, A., Lymar, E. S., Gamper, A. M., Kundu, T. K., Chait, B. T. and Roeder, R. G. (2001). Human STAGA complex is a chromatin-acetylating transcription coactivator that interacts with pre-mRNA splicing and DNA damage-binding factors in vivo. *Mol. Cell. Biol.* **21**, 6782-6795.

Maurer-Stroh, S., Dickens, N. J., Hughes-Davies, L., Kouzarides, T., Eisenhaber, F. and Ponting, C. P. (2003). The Tudor domain 'Royal Family': Tudor, plant Agenet, Chromo, PWWP and MBT domains. *Trends Biochem. Sci.* **28**, 69-74.

Melo, J. A., Cohen, J. and Toczyski, D. P. (2001). Two checkpoint complexes are independently recruited to sites of DNA damage in vivo. *Genes Dev.* **15**, 2809-2821.

Mirzoeva, O. K. and Petrini, J. H. (2001). DNA damage-dependent nuclear dynamics of the Mre11 complex. *Mol. Cell. Biol.* **21**, 281-288.

Mochan, T. A., Venere, M., DiTullio, R. A., Jr and Halazonetis, T. D. (2003). 53BP1 and NFBD1/MDC1-Nbs1 function in parallel interacting pathways activating ataxia-telangiectasia mutated (ATM) in response to DNA damage. *Cancer Res.* **63**, 8586-8591.

Mochida, S., Esashi, F., Aono, N., Tamai, K., O'Connell, M. J. and Yanagida, M. (2004). Regulation of checkpoint kinases through dynamic interaction with Crb2. *EMBO J.* **23**, 418-428.

Morales, J. C., Xia, Z., Lu, T., Aldrich, M. B., Wang, B., Rosales, C., Kellems, R. E., Hittelman, W. N., Elledge, S. J. and Carpenter, P. B. (2003). Role for the BRCA1 C-terminal repeats (BRCT) protein 53BP1 in maintaining genomic stability. *J. Biol. Chem.* **278**, 14971-14977.

Muchardt, C., Guilleme, M., Seeler, J. S., Trouche, D., Dejean, A. and Yaniv, M. (2002). Coordinated methyl and RNA binding is required for heterochromatin localization of mammalian HP1alpha. *EMBO Rep.* **3**, 975-981.

Nelms, B. E., Maser, R. S., MacKay, J. F., Lagally, M. G. and Petrini, J. H. (1998). In situ visualization of DNA double-strand break repair in human fibroblasts. *Science* **280**, 590-592.

Paull, T. T., Rogakou, E. P., Yamazaki, V., Kirchgessner, C. U., Gellert, M. and Bonner, W. M. (2000). A critical role for histone H2AX in recruitment of repair factors to nuclear foci after DNA damage. *Curr. Biol.* **10**, 886-895.

Paushkin, S., Gubitz, A. K., Massenet, S. and Dreyfuss, G. (2002). The SMN complex, an assemblyosome of ribonucleoproteins. *Curr. Opin. Cell Biol.* **14**, 305-312.

Ponting, C. P. (1997). Tudor domains in proteins that interact with RNA. *Trends Biochem. Sci.* **22**, 51-52.

Rappold, I., Iwabuchi, K., Date, T. and Chen, J. (2001). Tumor suppressor p53 binding protein 1 (53BP1) is involved in DNA damage-signaling pathways. *J. Cell. Biol.* **153**, 613-620.

Reits, E. A. and Neefjes, J. J. (2001). From fixed to FRAP: measuring protein mobility and activity in living cells. *Nat. Cell Biol.* **3**, E145-E147.

Ridanpaa, M., van Eenennaam, H., Pelin, K., Chadwick, R., Johnson, C., Yuan, B., vanVenrooij, W., Pruijn, G., Salmela, R., Rockas, S. et al. (2001). Mutations in the RNA component of RNase MRP cause a pleiotropic human disease, cartilage-hair hypoplasia. *Cell* **104**, 195-203.

Rodriguez, M., Yu, X., Chen, J. and Songyang, Z. (2003). Phosphopeptide binding specificities of BRCA1 COOH-terminal (BRCT) domains. *J. Biol. Chem.* **278**, 52914-52918.

Rogakou, E. P., Pilch, D. R., Orr, A. H., Ivanova, V. S. and Bonner, W. M. (1998). DNA double-stranded breaks induce histone H2AX phosphorylation on serine 139. *J. Biol. Chem.* **273**, 5858-5868.

Rogakou, E. P., Boon, C., Redon, C. and Bonner, W. M. (1999). Megabase chromatin domains involved in DNA double-strand breaks in vivo. *J. Cell Biol.* **146**, 905-916.

Saka, Y., Esashi, F., Matsusaka, T., Mochida, S. and Yanagida, M. (1997). Damage and replication checkpoint control in fission yeast is ensured by interactions of Crb2, a protein with BRCT motif, with Cut5 and Chk1. *Genes Dev.* **11**, 3387-3400.

Samejima, K. and Earnshaw, W. C. (2000). Differential localization of ICAD-L and ICAD-S in cells due to removal of a C-terminal NLS from ICAD-L by alternative splicing. *Exp. Cell Res.* **255**, 314-320.

Sanders, S. L., Portoso, M., Mata, J., Bahler, J., Allshire, R. C. and Kouzarides, T. (2004). Methylation of histone H4 lysine 20 controls recruitment of Crb2 to sites of DNA damage. *Cell* **119**, 603-614.

Schultz, L. B., Chehab, N. H., Malikzay, A. and Halazonetis, T. D. (2000). p53 binding protein 1 (53BP1) is an early participant in the cellular response to DNA double-strand breaks. *J. Cell Biol.* **151**, 1381-1390.

Schwartz, M. F., Duong, J. K., Sun, Z., Morrow, J. S., Pradhan, D. and Stern, D. F. (2002). Rad9 phosphorylation sites couple Rad53 to the Saccharomyces cerevisiae DNA damage checkpoint. *Mol. Cell* **9**, 1055-1065.

Soulier, J. and Lowndes, N. F. (1999). The BRCT domain of the S. cerevisiae checkpoint protein Rad9 mediates a Rad9-Rad9 interaction after DNA damage. *Curr. Biol.* **9**, 551-554.

Sprangers, R., Groves, M. R., Sinning, I. and Sattler, M. (2003). High-resolution X-ray and NMR structures of the SMN Tudor domain: conformational variation in the binding site for symmetrically dimethylated arginine residues. *J. Mol. Biol.* **327**, 507-520.

Volpe, T. A., Kidner, C., Hall, I. M., Teng, G., Grewal, S. I. and Martienssen, R. A. (2002). Regulation of heterochromatic silencing and histone H3 lysine-9 methylation by RNAi. *Science* **297**, 1833-1837.

Wang, B., Matsuoka, S., Carpenter, P. B. and Elledge, S. J. (2002). 53BP1, a Mediator of the DNA Damage Checkpoint. *Science* **298**, 1435-1438.

Ward, I. M., Minn, K., Jorda, K. G. and Chen, J. (2003a). Accumulation of checkpoint Protein 53BP1 at DNA breaks involves its binding to phosphorylated Histone H2AX. *J. Biol. Chem.* **278**, 19579-19582.

Ward, I. M., Minn, K., van Deursen, J. and Chen, J. (2003b). p53 Binding protein 53BP1 is required for DNA damage responses and tumor suppression in mice. *Mol. Cell. Biol.* **23**, 2556-25563.

Ward, J. F. (1998). Nature of lesions formed by ionizing radiation. In *DNA damage and repair, volume II: DNA repair in higher eukaryotes* (eds J. A. Nickoloff and M. F. Hoekstra), pp. 65-84. Totowa, New Jersey: Humana Press.

Yu, X., Chini, C. C., He, M., Mer, G. and Chen, J. (2003). The BRCT domain is a phospho-protein binding domain. *Science* **302**, 639-642.